



Presented at the NuMat 2010 Conference, 4–7 October 2010, Karlsruhe

## Density-functional study of U–Mo and U–Zr alloys

A. Landa\*, P. Söderlind, P.E.A. Turchi

Lawrence Livermore National Laboratory, Livermore, CA 94551, USA

### ARTICLE INFO

#### Article history:

Received 1 November 2010

Accepted 2 February 2011

Available online 13 February 2011

### ABSTRACT

The ground-state properties of U–Mo solid solutions are studied by density functional theory and compared to the similar U–Zr system. We discuss how the heat of formation in both alloys correlates with the charge transfer between the alloy components, and how the specific behavior of the density of states in the vicinity of the Fermi level promotes the stabilization of the  $U_2Mo$  compound. Our calculations suggest that, due to the existence of a single  $\gamma$ -phase over the typical fuel operation temperatures,  $\gamma$ -U–Mo alloys should indeed have much lower constituent redistribution than  $\gamma$ -U–Zr alloys for which binodal decomposition causes a high degree of constituent redistribution.

© 2011 Elsevier B.V. All rights reserved.

### 1. Introduction

Recently Kim et al. [1] published a paper suggesting some advantages of U–TRU–Mo fuels over U–TRU–Zr in TRU-burning advanced fast nuclear reactors (the abbreviation TRU states for ‘trans-uranium’): U–Pu–Mo fuels have higher thermal conductivity, lower thermal expansion, and higher melting points than U–Pu–Zr fuels resulting in advantages from a safety point of view; Mo is preferable to Zr because it is a stronger  $\gamma$ -stabilizer that provides stable swelling behavior in the case of U–Pu–Mo fuels; the higher density in U–Pu–Mo alloys allows for a somewhat more compact core design; and Mo has a lower reaction potential with the cladding (Fe) compared to Zr. However, the main advantages of U–TRU–Mo fuels lies in a much lower constituent redistribution, including migration of minor actinides (MA) and lanthanides toward the cladding due to the existence of a single  $\gamma$ -phase with body-centered cubic (bcc) structure over typical fuel operation temperatures (according to Ref. [2], U–Pu–Mo alloys exist in the single  $\gamma$ -phase field in the temperature range 550–950 °C). In contrast, U–Pu–Zr alloys extend over poly (three) phase fields in the temperature range 580–750 °C [2,3]. The difference in thermochemical properties between the adjoining phases in U–Pu–Zr fuels causes large chemical potential differences that originate from constituent redistribution (migration) and zone formation, although in U–Pu–Mo fuels only the radial-temperature gradient, which is much smaller than the chemical-potential gradient in U–Pu–Zr fuels, is responsible for this kind of migration. One should also remember that if MA Np is more uniformly distributed, much like Pu, in U–Pu–Zr alloys, MA Am redistribution is similar to that of Zr with tendency to precipitate to the center and near the fuel surface (cladding) where

large pores are observed [2–4]. As was mentioned in Ref. [4], the reaction of MA with the cladding leads to wall thinning and reduction of cladding melting point. If MA reacts with cladding, the cladding must be subject to reprocessing that increases the fuel cost [2–4]. All arguments presented so far indicate that replacing Zr with Mo in U–TRU–Zr fuels should bring significant benefits [1].

Low-enriched uranium alloys with 6–12 wt.% of Mo are under consideration by the Global Threat Reduction Initiative program [5] as very high density fuels (8–9 gU/cm<sup>3</sup> and 15–17 gU/cm<sup>3</sup> for dispersion-type and monolithic-type, respectively [6–8]) that allow nuclear research and test reactors conversion from use of highly-enriched uranium to low-enriched uranium fuels. Low-enriched uranium fuels are considered to be ~20% enriched that requires a large increase in fissile uranium per unit volume (the uranium density) to compensate for the reduction in enrichment [6,9–12]. U–Mo alloys are considered as the most prominent candidates for advanced research and test reactors because these alloys exhibit more stable irradiation performance when compared to other high density uranium alloys and compounds [10,12–14]. According to the U–Mo phase diagram [15], Mo exhibits a high solubility (~35 at.%) in  $\gamma$ -U (bcc) but below 560 °C the equilibrium state corresponds to a mixture of  $\alpha$ -U (orthorhombic) and so-called  $\gamma'$ -phase, which is the  $U_2Mo$  compound with the C11<sub>b</sub> (MoSi<sub>2</sub> prototype) structure. However, by rapid cooling from the  $\gamma$ -phase a metastable  $\gamma$ -state can be retained up to room temperature. There were numerous experimental studies performed on different U–Mo alloys, e.g., with 5.4 wt.% Mo [16], 7 wt.% Mo [17,18], 8 wt.% Mo [7], and 10 wt.% Mo [13,14,19,20].

Many experimental studies have been dedicated to U–Mo–Al(Si) alloys that serve as the basis for dispersion-type fuels. In these fuels the fuel material (U–Mo) is broken up into very small pieces that are dispersed into a matrix material (Al) [6]. The study of fuel–aluminum interactions, including interdiffusion, becomes an important issue in the analysis of the irradiation behavior, e.g.,

\* Corresponding author. Tel.: +1 925 424 3523; fax: +1 925 422 2851.

E-mail address: [landa1@llnl.gov](mailto:landa1@llnl.gov) (A. Landa).

the fuel swelling, as well as the growth rate and activation energy for the growth of reaction U–Mo/Al layers and their concentration profiles [18,21–25]. In order to reduce the interdiffusion and thus the interaction layer growth, an addition of some amount of Zr to the fuel and Si to the matrix have been recommended [26–29].

In spite of numerous experimental studies on U–Mo fuels very few theoretical efforts have been made to understand their behavior. According to Hofman et al. [30], the activation energy of nucleation during the decomposition of the metastable  $\gamma$ -U–Mo phase to  $\alpha$ -U and  $U_2Mo$  compound is proportional to the negative of the enthalpy of formation of the  $\gamma$ -U–Mo solid solutions. The excess thermodynamic functions of  $\gamma$ -U–Mo solid solutions were assessed from the experimental data available for this system by Vamberzkiy et al. [31] but their results were presented only graphically. Later, the integral quantities for U–Mo alloys, plotted in Ref. [31], have been summarized and tabulated in Ref. [32]. As one can note from Fig. 11 of Ref. [31], the enthalpy of formation of  $\gamma$ -U–Mo solid solutions is positive in a larger fraction of the composition interval of the U–Mo phase diagram but changes its sign from positive to negative when uranium concentration exceeds  $\sim 85$  at.%. One should note that the assessment [31] was performed at a very high temperature,  $T = 1100$  K. Parida et al. [33] compiled experimental data on the excess thermodynamic functions of the quenched (below the temperature of the stable  $\gamma$ -region)  $U_{0.823}Mo_{0.177}$  and  $U_{0.94}Mo_{0.06}$  alloys and presented the measured enthalpy increment values in a polynomial form in the temperature range from 299 to 820 K.

So far there has only been one attempt [34] to perform *ab initio* study of the formation energy of  $\gamma$ -U–Mo solid solutions. Using the cluster expansion technique within the Ising Hamiltonian formalism with a set of effective cluster interactions defined by the direct inversion method from the total energies of 16 bcc-based ordered structures calculated by the full-potential linearized augmented-plane-wave method, these authors calculated the formation energy of the disordered  $\gamma$ -U–Mo solid solutions as well as the  $U_2Mo$  ( $C11_b$ ) compound. These calculations proved that the  $U_2Mo$  compound is stable (has a negative formation energy) and the disordered  $\gamma$ -U–Mo solid alloys should be stable on the uranium rich side of the phase diagram (the formation energy of  $\gamma$ -U–Mo solid solutions changes the sign from positive to negative when uranium composition exceeds  $\sim 70$  at.%). However, temperatures of calculated phase equilibria were excessively high, e.g., the calculated temperature of disordering of the  $U_2Mo$  ( $C11_b$ ) compound is  $\sim 2000$  °C, which is much higher than the experimental value of  $\sim 600$  °C [15]. This failure indicates that a more accurate *ab initio* technique should be selected to study phase equilibria in U–Mo system.

Semi-empirical model calculations [35], supported by experimental observations, indicate that the excess enthalpy of solution of  $\gamma$ -U–Zr phase controls the constituent redistribution process in U–Zr fuels. This statement encouraged us to perform successful *ab initio* calculations of the heat of formation of  $\gamma$ -U–Zr solid solutions as well as to study the nature of the formation of the  $\delta$ -U–Zr<sub>2</sub> ( $C32$ ) compound [36,37]. We later expanded our study to the ternary U–Pu–Zr system [38], which is considered as a candidate metallic nuclear fuel for fast breeder reactors, as well as to the bcc alloys that plutonium forms with MA (neptunium, americium, and curium) [39]. In the present study we report similar calculations for U–Mo alloys and compare our results with previous results obtained for U–Zr alloys. The purpose of this study is not only to provide theoretical estimation of the main thermodynamic characteristics of U–Mo alloys but also to bring to light the nature of the difference in constituent redistributions in U–Mo and U–Zr fuels.

For our calculations we employ two complementary computational techniques: (i) the exact muffin-tin orbital method (EMTO)

and (ii) the full-potential linear muffin-tin orbital method (FPLMTO). Pertinent details of the computational methods are described in Section 2. Results of the density-functional calculations of the ground-state properties of U–Zr and U–Mo solid solutions are presented in Section 3. We provide discussion in Section 4. Lastly, concluding remarks are presented in Section 5.

## 2. Computational details

The calculations we have referred to as EMTO are performed using the scalar-relativistic (SR) Green's-function technique based on the improved screened Korringa–Kohn–Rostoker (KKR) method, where the one-electron potential is represented by optimized overlapping muffin-tin (OOMT) potential spheres [40,41]. Inside the potential spheres the potential is spherically symmetric, and it is constant between the spheres. The radii of the potential spheres, the spherical potentials inside the spheres, and the constant value in the interstitial region are determined by minimizing (i) the deviation between the exact and overlapping potentials, and (ii) the errors caused by the overlap between the spheres. Within the EMTO formalism, the one-electron states are calculated exactly for the OOMT potentials. As an output of the EMTO calculations, one can determine the self-consistent Green's-function of the system and the complete, non-spherically symmetric charge density. Finally, the total energy is calculated using the full charge-density technique [42]. The calculations are performed for a basis set including valence *spdf* orbitals. For the electron exchange and correlation energy functional, the generalized gradient approximation (GGA) is considered [43]. Integration over the Brillouin zone is performed using the special *k* point technique [44] with 506 points and 1470 points in the irreducible wedge of the Brillouin zone for the bcc and  $C11_b$  structures, respectively. The moments of the density of states, needed for the kinetic energy and the valence charge density, are calculated by integrating the Green's-function over a complex energy contour (with a 3.0 Ry diameter) using a Gaussian integration technique with 40 points on a semi-circle enclosing the occupied states.

To treat compositional disorder the EMTO method is combined with the coherent potential approximation (CPA) [45,46]. The ground-state properties of the chemically random U–Mo alloys are obtained from SR-EMTO-CPA calculations that include the Coulomb screening potential and energy [47–49]. The screening constants are determined from supercell calculations using the locally self-consistent Green's-function (LSGF) method [50] for a 1024 atoms supercell that models the random equiatomic alloy. The  $\alpha$  and  $\beta$  screening constants (see Refs. [47,48] for details) are found to be 0.725 and 1.088 for U–Mo alloys. The equilibrium atomic density of U–Mo alloys is obtained from a Murnaghan fit to the total energy vs. lattice constant curve [51].

For the elemental metals, the most accurate calculations are performed using a full-potential (no geometrical approximations) approach. These are fully-relativistic in the sense that spin–orbit interaction is accounted for through the conventional perturbative scheme [52] that has the accuracy of solving the Dirac equation for the light actinides [53]. Although unable to model disorder in the CPA sense it provides important information for the metals, and also serves to confirm the CPA calculations mentioned above. For this purpose we use a version of the FPLMTO [54] and the “full-potential” (FP) in FPLMTO refers to the use of non-spherical contributions to the electron charge density and potential. This is accomplished by expanding the charge density and potential in cubic harmonics inside non-overlapping muffin-tin spheres and in a Fourier series in the interstitial region. We use two energy tails associated with each basis orbital, and for U's semi-core 6s, 6p states and valence states (7s, 7p, 6d, and 5f) these pairs are differ-

ent. With this ‘double basis’ approach we use a total of six energy tail parameters and a total of 12 basis functions per atom. Spherical harmonic expansions are carried out up to  $l_{max} = 6$  for the basis, potential, and charge density. As in the case of the EMT method, GGA is used for the electron exchange–correlation approximation. Finally, a special quasi-random structure (SQS) method, utilizing a 16-atom supercell, was used to treat the compositional disorder within the FPLMTO formalism [55].

### 3. Ground-state properties of U–Zr and U–Mo solid solutions

Fig. 1a shows results of our previous SR-KKR-ASA-CPA calculations of the heat of formation of  $\gamma$ -U–Zr solid solutions at  $T = 0$  K [37]. The abbreviation KKR-ASA implies a Green’s-function technique based on the KKR method within the atomic sphere approximation (ASA) [56–59]. The heat of formation, that shows a positive deviation from the energy associated with a mixture of the pure elements, agrees well with the existence of a miscibility gap in the U–Zr phase diagram. Notice that the calculated heat of formation of  $\gamma$ -U–Zr solid solutions is in excellent agreement with data derived from a CALPHAD assessment [60–62] of the experimental thermodynamics and phase diagram information, which validates the *ab initio* approach. Note that to have a consistent comparison between the *ab initio* and CALPHAD results, the heat of formation within CALPHAD is extrapolated at  $T = 0$  K. For comparison, we also show the heats of formation for  $U_{75}Zr_{25}$ ,  $U_{50}Zr_{50}$ , and  $U_{25}Zr_{75}$  bcc alloys, calculated within the FPLMTO-SQS technique that agrees pretty well with both SR-KKR-ASA-CPA and CALPHAD assessment results.

Fig. 1b show results of present SR-EMTO-CPA calculations of the heat of formation of  $\gamma$ -U–Mo solid solutions at  $T = 0$  K. The calculated heat of formation is positive in a broad region of the composition interval of the U–Mo phase diagram but changes its sign from positive to negative when uranium composition exceeds  $\sim 80$  at.%. For comparison, we also show the heats of formation for  $U_{75}Mo_{25}$ ,  $U_{50}Mo_{50}$ , and  $U_{25}Mo_{75}$  bcc alloys, calculated within the FPLMTO-SQS technique that agrees pretty well with SR-EMTO-CPA results. This plot also shows results of calculations of the heat of formation of the  $U_2Mo$  (C11<sub>b</sub>) compound relative to the bcc-based U and Mo components, and these results are almost identical for both SR-EMTO and FPLMTO-SQS methods. A good agreement between the results derived by different methods suggests a robustness of the

*ab initio* approaches, especially of the SR-EMTO-CPA method that is selected to treat disordered  $\gamma$ -U–Mo solid solutions.

Fig. 2a and b shows results of calculations of the equilibrium atomic volume versus composition of the bcc U–Zr and U–Mo alloys at  $T = 0$  K. There is a positive deviation from Vegard’s law for  $\gamma$ -U–Zr alloys (results of SR-KKR-ASA-CPA calculations [37]) that is in accord with the positive heat of formation in this system. Results of SR-EMTO-CPA calculations for  $\gamma$ -U–Mo alloys, shown in this figure, indicate a slight positive deviation from Vegard’s law with a visible inflection around the  $U_2Mo$  compound stoichiometry.

In Fig. 3 we compare the results of the present SR-EMTO-CPA calculations of the heat of formation of  $\gamma$ -U–Mo solid solutions with those obtained in Ref. [34]. The formation energies of the  $U_2Mo$  (C11<sub>b</sub>) compound relative to bcc U and Mo metals are also compared. From this figure it is clearly seen that comparison of the present SR-EMTO-CPA and the cluster expansion [34] results shows that the results of the SR-EMTO-CPA calculations for the disordered  $\gamma$ -U–Mo solid solutions show smaller variation and magnitude, and the absolute value of the heat of formation of the  $U_2Mo$  (C11<sub>b</sub>) compound is almost twice smaller than the one calculated with the cluster expansion technique [34]. This comparison encourages us to believe the SR-EMTO database should allow us to reproduce the U–Mo phase diagram with a much higher accuracy than was done in Ref. [34].

### 4. Discussion

Within the EMT formalism [40,41], the total-energy,  $E_{tot}$ , can be expressed as the sum of two contributions:  $E_{tot} = E_b + E_M$ , where  $E_b$  consists of all “local” (band-structure) contributions,  $E_b = E_s + E_{intra} + E_{xc}$ , such as the kinetic energy of non-interacting electron gas,  $E_s$ , the intra-cell electrostatic energy,  $E_{intra}$ , which is due to the electron–electron and electron–ion Coulomb interactions, and the exchange and correlation energy,  $E_{xc}$ . The remaining contribution,  $E_M$ , is the inter-cell Madelung energy. A similar decomposition of the total energy is possible within the KKR-ASA formalism.

In the Table 1 we compare the results of our calculated heat of formation,  $\Delta E_{tot}$ , of bcc  $U_{50}Mo_{50}$  and  $U_{50}Zr_{50}$  alloys. This Table also lists the energy contributions,  $\Delta E_b$ , and  $\Delta E_M$ , the equilibrium Wigner–Seitz radius,  $S_{WS}$ , (the volume of a sphere with this radius equals the atomic volume), the screening constants,  $\alpha$  and  $\beta$ , and the charge transfer from U atoms,  $\Delta Q_U$ , that is calculated by the

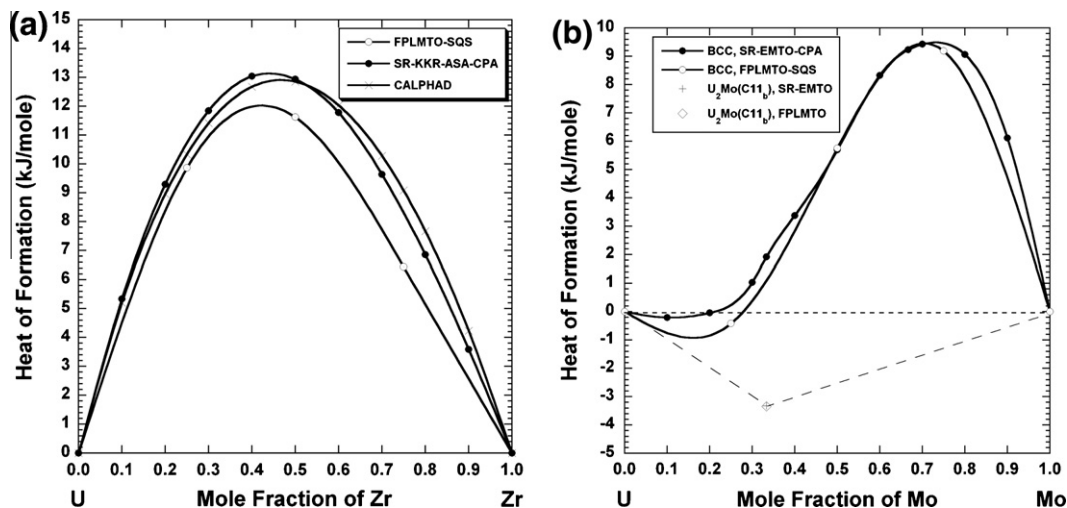


Fig. 1. The heat of formation versus composition calculated at  $T = 0$  K for: (a)  $\gamma$ -U–Zr [37] and (b)  $\gamma$ -U–Mo alloys; and (b) the heat of formation calculated at  $T = 0$  K for the  $U_2Mo$  (C11<sub>b</sub>) compound relative to bcc U and Mo. The full lines are guides to the eye only.

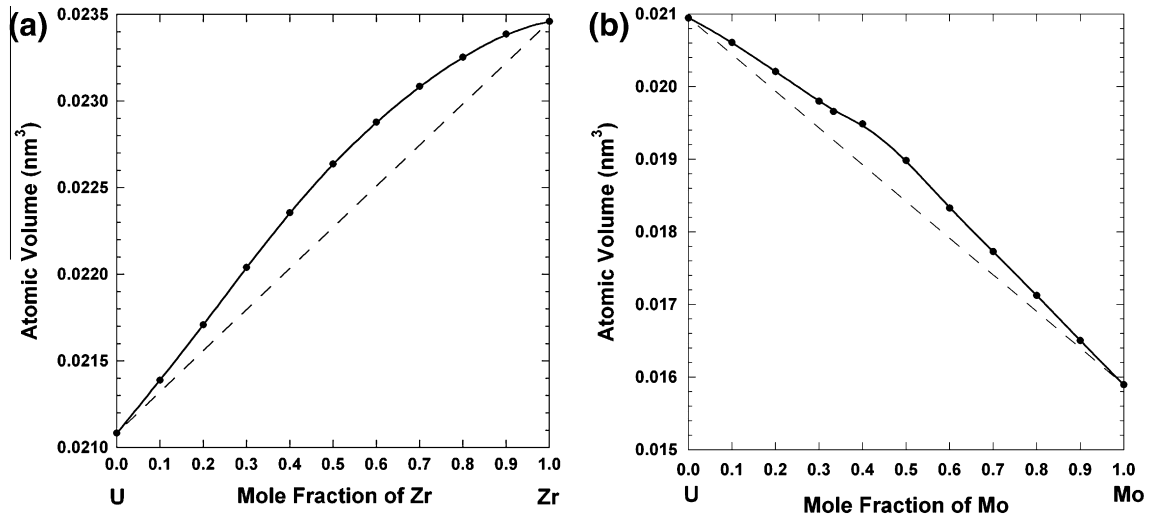


Fig. 2. The atomic volume versus composition calculated at  $T = 0$  K for (a)  $\gamma$ -U-Zr [38] and (b)  $\gamma$ -U-Mo alloys. The full lines are guides to the eye only.

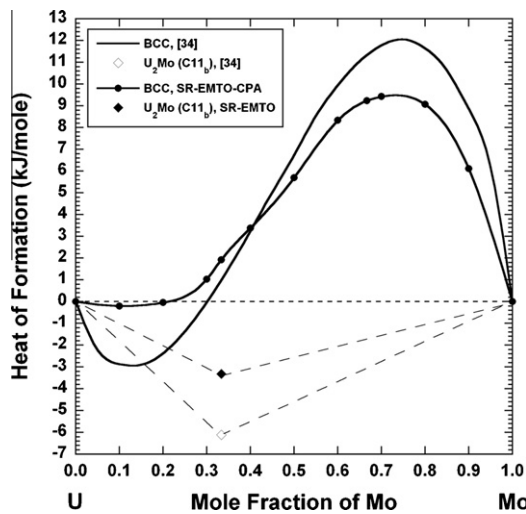


Fig. 3. The heat of formation versus composition calculated at  $T = 0$  K for  $\gamma$ -U-Mo alloys and the heat of formation calculated at  $T = 0$  K for the  $U_2Mo$  ( $C11_u$ ) compound relative to bcc U and Mo. Results of previous calculations [34] are also shown. In the case of SR-EMTO-CPA calculations, the full line is guide to the eye only.

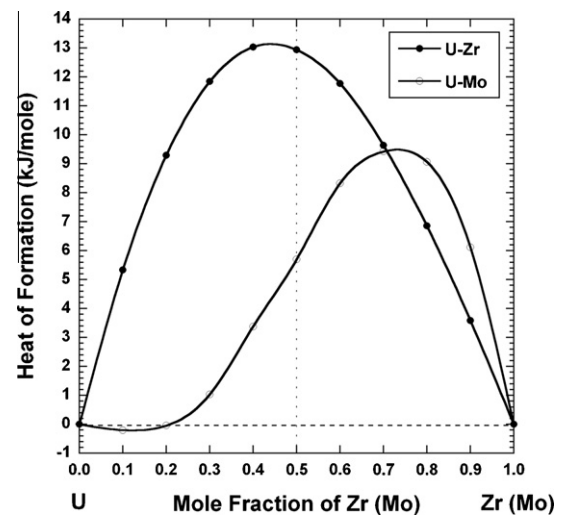


Fig. 4. The heat of formation versus composition calculated at  $T = 0$  K for  $\gamma$ -U-Zr and  $\gamma$ -U-Mo alloys. The full lines are guides to the eye only.

Table 1

Equilibrium Wigner-Seitz radius,  $S_{WS}$ , (in a.u., 1 a.u. = 0.0529 nm), screening constants,  $\alpha$  and  $\beta$ , charge transfer from U atoms,  $\Delta Q_U$ , contributions,  $\Delta E_b$  and  $\Delta E_M$ , to the heat of formation,  $\Delta E_{tot}$ , (in kJ/mole) of the bcc  $U_{50}Mo_{50}$  and  $U_{50}Zr_{50}$  alloys. The screening constants for the  $U_{50}Zr_{50}$  alloy are taken from Ref. [36].

Alloy	$S_{WS}$	$\alpha$	$\beta$	$\Delta Q_U$	$\Delta E_b$	$\Delta E_M$	$\Delta E_{tot}$
$U_{50}Mo_{50}$	3.1274	0.725	1.088	-0.440	74.5648	-68.8681	5.6967
$U_{50}Zr_{50}$	3.3163	0.700	1.060	-0.248	32.4705	-19.5332	12.9373

LSGF method for a 1024 atoms supercell that models the random equiatomic alloy. According to Ref. [48], the Madelung energy contribution to the heat of formation of a disordered  $A_cB_{1-c}$  alloy is proportional to  $(-\alpha \frac{(\Delta Q)^2}{S_{WS}} \beta c(1-c))$ , where  $c$  is the concentration of the component 'A'. The Madelung energy contribution to the heat of formation of a disordered alloy is always negative and, as one can see from the Table 1, the absolute value of this contribution for the  $U_{50}Mo_{50}$  alloy is  $\sim 3.53$  larger than for the  $U_{50}Zr_{50}$  alloy (one can also simple estimate this ratio using the input data listed in the Table 1 and above mentioned expression). This ponderable negative Madelung energy contribution to the heat of formation

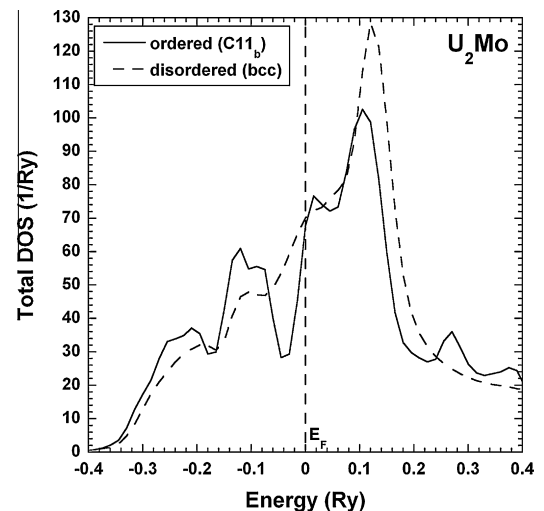


Fig. 5. The DOS versus energy calculated for the U-Mo system (the Fermi energy is selected as zero energy).



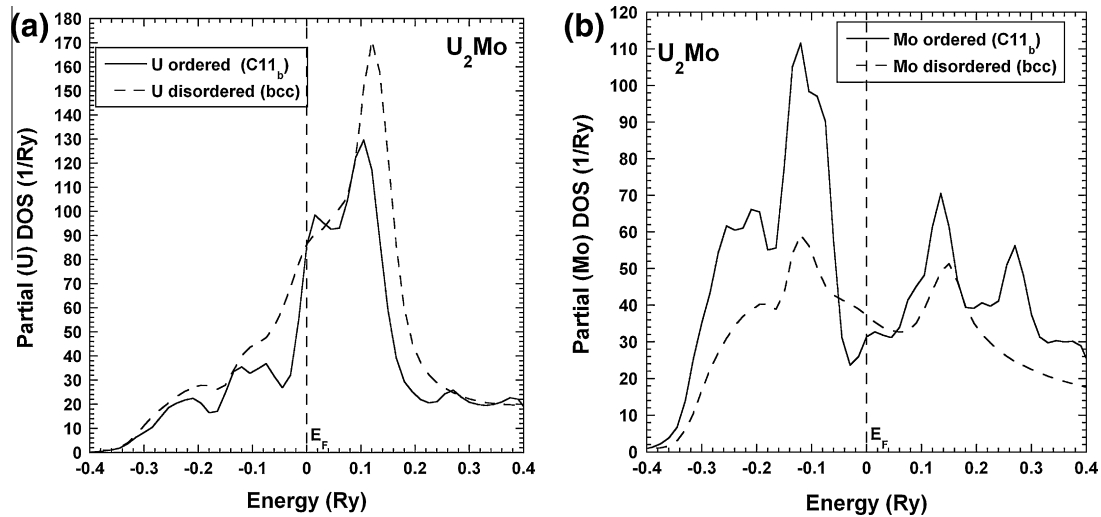


Fig. 6. The partial DOS versus energy of (a) U and (b) Mo calculated for the U-Mo system (the Fermi energy is selected as zero energy).

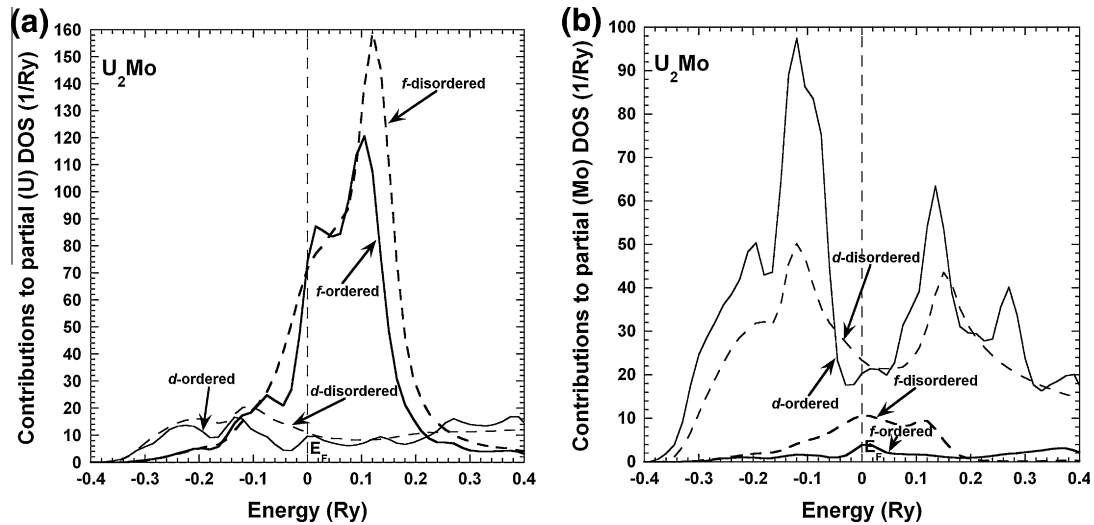


Fig. 7. The contributions to the partial DOS versus energy of (a) U and (b) Mo calculated for the U-Mo system (the Fermi energy is selected as zero energy).

of the  $U_{50}Mo_{50}$  alloy in comparison with one for the  $U_{50}Zr_{50}$  alloy is predominantly due to a significantly larger absolute value of the charge transfer from U atoms in the case of U-Mo alloys than in the case of U-Zr alloys (U has a larger Wigner-Seitz radius than Mo but smaller than Zr). Even the band-structure contribution to the heat of formation,  $\Delta E_b$ , is positive and  $\sim 2.30$  larger for the  $U_{50}Mo_{50}$  alloy than for the  $U_{50}Zr_{50}$  alloy, the large negative Madelung energy contribution prevails in the case of the  $U_{50}Mo_{50}$  alloy resulting in a drop of the heat of formation of this alloy by the factor of  $\sim 2.27$  in comparison with the  $U_{50}Zr_{50}$  alloy.

In Fig. 4 we compared the results of our calculations of the heat of formation of bcc U-Zr and U-Mo solid solutions within the whole concentration interval. By comparing the heats of formation for these alloys one can explain why decomposition takes place in the case of  $\gamma$ -U-Zr alloys that causes much higher constituent redistribution in U-TRA-Zr fuels than in U-TRA-Mo fuels where a single  $\gamma$ -phase field exists.

In order to explain why the disordered  $\gamma$ - $U_2Mo$  alloy is unstable with respect to the ordering to the  $U_2Mo$  (C11<sub>b</sub>) structure, we plot the total electronic density of states (DOS) for this disordered and ordered  $U_2Mo$  alloy (Fig. 5). One can see that there is a significant drop of the DOS in the vicinity of the Fermi level ( $E_F$ ) in the case of

the ordered (C11<sub>b</sub>) compound that causes a decrease of the band-structure contribution ( $E_b$ ) to the total energy. Fig. 6a and b shows the partial contributions to the total DOS from U and Mo, respectively. For both components of U-Mo alloys a similar drop of the partial DOS is also observed. In order to understand which electrons contribute to this phenomenon, we show contributions to the partial DOS of U and Mo in Fig. 7a and b, respectively. It is not surprising to find that *f*-electrons play the major role in the U-partial DOS and similarly that *d*-electrons play the major role in the Mo-partial DOS when ordering and formation of the C11<sub>b</sub> structure takes place. The *s*- and *p*-contributions to the partial DOS of U and Mo are negligible in the vicinity of the Fermi level and not shown in Fig. 7a and b.

## 5. Conclusion

In the present paper *ab initio* results are obtained for U-Mo alloys to understand the effectiveness of the first-principle methods in describing actinide alloys that could be used as very promising fuels for TRU-burning fast reactors. We consider that the calculated heats of formation for the  $\gamma$ -U-Mo solid solutions and the  $U_2Mo$

(C11<sub>b</sub>) compound are based on an electron behavior, which is well understood, and can be used for future calculations of the U–Mo phase diagram. Our calculations suggest the physical origin of a very weak constituent redistribution in  $\gamma$ -U–Mo fuels in comparison with their  $\gamma$ -U–Zr counterparts as well as the nature of formation of the U<sub>2</sub>Mo ordered compound. In the future we plan to perform similar calculations for U–Mo fuels doped with some amount of Al, Si, and Zr in order to study interdiffusion process [21–29] in U–Mo-based dispersion fuels. *Ab initio* calculations for U–Mo–Zr alloys could be also important for estimation of a Zr diffusion barrier recently studied in U–Mo-based monolithic fuels [8]. These *ab initio* results will be used to build a thermodynamic database with important input from first-principles theory that will be directly comparable to the results obtained solely from experimental data on thermodynamic properties and phase diagrams.

## Acknowledgement

This work was performed under the auspices of the US Department of Energy by Lawrence Livermore National Laboratory under contract DE-AC52-07NA27344.

## References

- [1] Y.-S. Kim, G.L. Hofman, A.M. Yacout, T.-K. Kim, in: T. Okazaki, J. Bouchard, T. Takeda, Y. Oka (Eds.), Proceedings of International Conference on Fast Reactors and Related Fuel Cycles (FR09), Challenges and Opportunities, IAEA-CN-176, Kyoto, Japan, 2009, pp. 1–9.
- [2] Y.-S. Kim, G.L. Hofman, A.M. Yacout, J. Nucl. Mater. 392 (2009) 164.
- [3] Y.-S. Kim, S.L. Hayes, G.L. Hofman, A.M. Yacout, J. Nucl. Mater. 359 (2006) 17.
- [4] Y.-S. Kim, G.L. Hofman, S.L. Hayes, Y.-H. Sohn, J. Nucl. Mater. 327 (2004) 27.
- [5] P. Staples, in: Transactions of 14th International Topical Meeting on Research Reactor Fuel Management (RRFM 2010), ENS-IAEA, Marrakech, Morocco (2010), Session 1, pp. 1–6.
- [6] D.M. Wachs, Nuclear Engineering International, 08 March 2010, pp. 1–6.
- [7] R.M. Hengstler, L. Beck, H. Breitzkreutz, C. Jarousse, R. Jungwirth, W. Petry, W. Schmid, J. Schneider, N. Weischalla, J. Nucl. Mater. 402 (2010) 74.
- [8] E. Perez, B. Yao, D.D. Keiser Jr., Y.-H. Sohn, J. Nucl. Mater. 402 (2010) 8.
- [9] J.H. Kittel, B.R.T. Frost, J.P. Mustelier, K.Q. Bagley, G.C. Crittenden, J. Van Dievoet, J. Nucl. Mater. 204 (1993) 1.
- [10] J.L. Snelgrove, G.L. Hofman, M.K. Meyer, C.L. Trybus, T.C. Wiencek, Nucl. Eng. Des. 178 (1997) 119.
- [11] K.-H. Kim, D.-B. Lee, C.-K. Kim, G.E. Hofman, K.-W. Paik, J. Nucl. Mater. 245 (1997) 179.
- [12] M.K. Meyer, G.L. Hofman, S.L. Hayes, C.R. Clark, T.C. Wiencek, J.L. Snelgrove, R.V. Strain, K.-H. Kim, J. Nucl. Mater. 304 (2002) 221.
- [13] J.-M. Park, H.-J. Ryu, K.-H. Kim, D.-B. Lee, Y.-S. Lee, J.-S. Lee, B.-S. Seong, C.-K. Kim, M. Cornen, J. Nucl. Mater. 397 (2010) 27.
- [14] D.E. Burkes, C.A. Papesch, A.P. Maddison, T. Hartmann, F.J. Rice, J. Nucl. Mater. 403 (2010) 160.
- [15] H. Okamoto, in: T.B. Massalski (Ed.), Binary Alloys Phase Diagrams, second ed., vol. 3, ASM International, Materials Park, Ohio, 1990, p. 2682.
- [16] J.-S. Lee, C.-H. Lee, K.-H. Kim, V. Em, J. Nucl. Mater. 280 (2000) 116.
- [17] A. Leenaers, S. Van den Berghe, E. Koonen, C. Jarousse, F. Huet, M. Trotabas, M. Boyard, S. Guillot, L. Sannen, M. Verwert, J. Nucl. Mater. 335 (2004) 39.
- [18] S. Van den Berghe, W. Van Renterghem, A. Leenaers, J. Nucl. Mater. 375 (2008) 340.
- [19] B.-S. Seong, C.-H. Lee, J.-S. Lee, H.-S. Shim, J.-H. Lee, K.-H. Kim, C.-K. Kim, V. Em, J. Nucl. Mater. 277 (2000) 274.
- [20] V.P. Sinha, G.L. Prasad, P.V. Hedge, R. Keswani, C.B. Basak, S. Pal, G.P. Mishra, J. Alloys Compd. 473 (2009) 238.
- [21] G.L. Hofman, J.L. Snelgrove, S.L. Hayes, M.K. Meyer, in: P. Gubel (Ed.), Transactions of the 6th International Topical Meeting on Research Reactor Fuel Management (RRFM 2002), ENS-IAEA, Ghent, Belgium, 2002, pp. 50–58.
- [22] H.-J. Ryu, Y.-S. Han, J.-M. Park, S.-D. Park, C.-K. Kim, J. Nucl. Mater. 321 (2003) 210.
- [23] F. Mazaudier, C. Proye, F. Hodaj, J. Nucl. Mater. 377 (2008) 476.
- [24] H. Palancher, N. Wieschalla, P. Martin, R. Tucoulou, C. Sabathier, W. Petry, J.-F. Berar, C. Valot, S. Dubois, J. Nucl. Mater. 385 (2009) 449.
- [25] H.-J. Ryu, Y.-S. Kim, G.L. Hofman, J. Nucl. Mater. 385 (2009) 623.
- [26] J.-M. Park, H.-J. Ryu, S.-J. Oh, D.-B. Lee, C.-K. Kim, Y.-S. Kim, G.L. Hofman, J. Nucl. Mater. 374 (2008) 422.
- [27] M. Mirandou, S. Arico, M. Rosenbusch, M. Ortiz, S. Balart, L. Gribaudo, J. Nucl. Mater. 384 (2009) 268.
- [28] D.D. Keiser Jr., A.B. Robinson, J.-F. Jue, P. Medvedev, D.M. Wachs, M.R. Finlay, J. Nucl. Mater. 393 (2009) 311.
- [29] J. Gan, D.D. Keiser Jr., D.M. Wachs, A.B. Robinson, B.D. Miller, T.R. Allen, J. Nucl. Mater. 396 (2010) 234.
- [30] G.L. Hofman, M.K. Meyer, A.R. Ray, in: A. Travelli (Ed.), Proceedings of the 21st International Meeting on Reduced Enrichment for Research and Test Reactors (1998 RERTR), ANL, San Paulo, Brazil, 1998, 12 p.
- [31] Yu.V. Vamberskiy, A.L. Udovskiy, O.S. Ivanov, J. Nucl. Mater. 46 (9) (1973) 192.
- [32] P. Chiotti, V.V. Akhachinskij, I. Ansara, M.H. Rand, The Chemical Thermodynamics of Actinide Elements and Compounds, Part 5, The Actinide Binary Alloys, IAEA, Vienna, 1981, 145.
- [33] S.C. Parida, S. Dash, Z. Singh, R. Prasad, V. Venugopal, J. Phys. Chem. Sol. 62 (2001) 585.
- [34] P.R. Alonso, G.H. Rubiolo, Model. Simul. Mater. Sci. Eng. 15 (2007) 263.
- [35] G.L. Hofman, S.L. Hayes, M.C. Petri, J. Nucl. Mater. 227 (1996) 277.
- [36] A. Landa, P. Söderlind, P.E.A. Turchi, J. Alloys Compd. 478 (2009) 103.
- [37] A. Landa, P. Söderlind, P.E.A. Turchi, L. Vitos, A. Ruban, J. Nucl. Mater. 385 (2009) 68.
- [38] A. Landa, P. Söderlind, P.E.A. Turchi, L. Vitos, A. Ruban, J. Nucl. Mater. 393 (2009) 141.
- [39] A. Landa, P. Söderlind, P.E.A. Turchi, L. Vitos, O.E. Peil, A.V. Ruban, J. Nucl. Mater. 408 (2011) 61.
- [40] L. Vitos, Phys. Rev. B 64 (2001) 014107.
- [41] L. Vitos, Computational Quantum Mechanics for Materials Engineers: The EMT Method and Application, Springer, London, 2007.
- [42] J. Kollar, L. Vitos, H.L. Skriver, in: H. Dreyssé (Ed.), Electronic Structure and Physical Properties of Solids: The Uses of the LMTO Method, Lecture Notes in Physics, Springer, Berlin, 2000, pp. 85–113.
- [43] J.P. Perdew, K. Burke, M. Ernzerhof, Phys. Rev. Lett. 77 (1996) 3865.
- [44] D.J. Chadi, M.L. Cohen, Phys. Rev. B 8 (1973) 5747; S. Froyen, Ibid 39 (1989) 3168.
- [45] J.S. Faulkner, Prog. Mater. Sci. 27 (1982) 1.
- [46] L. Vitos, I.A. Abrikosov, B. Johansson, Phys. Rev. Lett. 87 (2001) 156401.
- [47] A.V. Ruban, H.L. Skriver, Phys. Rev. B 66 (2002) 024201.
- [48] A.V. Ruban, S.I. Simak, P.A. Korzhavyi, H.L. Skriver, Phys. Rev. B 66 (2002) 024202.
- [49] A.V. Ruban, S.I. Simak, S. Shallcross, H.L. Skriver, Phys. Rev. B 67 (2003) 214302.
- [50] I.A. Abrikosov, S.I. Simak, B. Johansson, A.V. Ruban, H.L. Skriver, Phys. Rev. B 56 (1997) 9319.
- [51] F.D. Murnaghan, Natl. Acad. Sci. USA 30 (1944) 244.
- [52] O.K. Andersen, Phys. Rev. B 12 (1975) 3060.
- [53] A. Landa, P. Söderlind, in: J.L. Sarrao, A.J. Schwartz, M.R. Antonio, P.C. Burns, R.G. Haire, H. Nitsche (Eds.), Actinides 2005–Basic Science, Applications and Technology, Material Research Society, Warrendale, vol. 893, 2006, pp. 51–56.
- [54] J.M. Wills, O. Eriksson, M. Alouani, D.L. Price, in: H. Dreyssé (Ed.), Electronic Structure and Physical Properties of Solids: The Uses of the LMTO Method, Lecture Notes in Physics, Springer, Berlin, 2000, pp. 148–167.
- [55] A. Zunger, S.H. Wei, L.G. Ferreira, J.E. Bernard, Phys. Rev. Lett. 65 (1990) 353.
- [56] O. Gunnarsson, O. Jepsen, O.K. Andersen, Phys. Rev. B 27 (1983) 7144.
- [57] I.A. Abrikosov, H.L. Skriver, Phys. Rev. B 47 (1993) 16532.
- [58] A.V. Ruban, H.L. Skriver, Comput. Mater. Sci. 15 (1999) 119.
- [59] N.E. Christensen, S. Satpathy, Phys. Rev. Lett. 55 (1985) 600.
- [60] P.E.A. Turchi, I.A. Abrikosov, B. Burton, S.G. Fries, G. Grimvall, L. Kauffman, P. Korzhavyi, V. Rao Manga, M. Ohno, A. Pisch, A. Scott, W. Zhang, CALPHAD 31 (2007) 4.
- [61] M. Kurata, T. Ogata, K. Nakamura, T. Ogawa, J. Alloys Compd. 271/273 (1998) 636.
- [62] M. Kurata, CALPHAD 23 (1999) 315.